Structural Analysis of the Phototactic Transducer Protein HtrII Linker Region from *Natronomonas pharaonis*[†,‡]

Kokoro Hayashi,[§] Yuki Sudo,[||,⊥] JunGoo Jee,[§] Masaki Mishima,[§] Hideyuki Hara,[@] Naoki Kamo,[||] and Chojiro Kojima*[,§]

Laboratory of Biophysics, Graduate School of Biological Sciences, Nara Institute of Science and Technology (NAIST), 8916-5 Takayama, Ikoma, Nara 630-0192, Japan, Laboratory of Biophysical Chemistry, Graduate School of Pharmaceutical Sciences and Faculty of Advanced Life Sciences, Hokkaido University, Sapporo 060-0812, Japan, and ESR Division of Bruker Biospin K. K., Tsukuba, Ibaraki 305-0051, Japan

Received September 8, 2007; Revised Manuscript Received October 16, 2007

ABSTRACT: Halobacterial *pharaonis* phoborhodopsin [*p*pR, also called *Natronomonas pharaonis* sensory rhodopsin II (*Np*SRII)] is a phototaxis protein which transmits a light signal to the cytoplasm through its transducer protein (*p*HtrII). *p*HtrII, a two-transmembrane protein that interacts with *p*pR, belongs to the group of methyl-accepting chemotaxis proteins (MCPs). Several mutation studies have indicated that the linker region connecting the transmembrane and methylation regions is necessary for signal transduction. However, the three-dimensional (3D) structure of an MCP linker region has yet to be reported, and hence, details concerning the signal transduction mechanism remain unknown. Here the structure of the *p*HtrII linker region was investigated biochemically and biophysically. Following limited proteolysis, only one trypsin resistant fragment in the *p*HtrII linker region was identified. This fragment forms a homodimer with a K_d value of 115 μM. The 3D structure of this fragment was determined by solution NMR, and only one α-helix was found between two HAMP domains of the linker region. This α-helix was significantly stabilized within transmembrane protein *p*HtrII as revealed by CW-EPR. The presence of Af1503 HAMP domain-like structures in the linker region was supported by CD, NMR, and ELDOR data. The α-helix determined here presumably works as a mechanical joint between two HAMP domains in the linker region to transfer the photoactivated conformational change downstream.

Transducer protein *p*HtrII from the extreme halophilic and alkalophilic archaeon *Natronomonas pharaonis* is a two-transmembrane protein, belonging to the group of methyl-accepting chemotaxis proteins (MCPs)[1] (*1*), forms a homodimer comprising subunits of ca. 60 kDa, and is located in the cytoplasmic membrane. MCPs form a complex with the histidine kinase CheA and the adaptor protein CheW. The stimuli associated with this group of proteins modulate the flagella motors via phosphorylation cascades (*2*−*5*). In bacterial chemotactic signal transduction, MCPs act as transducers as well as signal receptors, whereas phototactic signaling in *N. pharaonis* utilizes *p*HtrII in the form of a complex with photosignal receptor *pharaonis* phoborhodopsin, *p*pR [also called *N. pharaonis* sensory rhodopsin II (*Np*SRII)] (*6*). *p*pR is a member of the seven-transmembrane helical retinal binding protein family which includes rhodopsin and bacteriorhodopsin (*7*). M and/or O photo intermediate states of *p*pR activate signal transduction through *p*HtrII (*8*, *9*).

*p*HtrII consists of four distinct areas comprising transmembrane, linker, methylation, and signaling regions (Figure 1). Crystal structures of the two-transmembrane region of *p*HtrII comprising residues 24−82 as complexes with *p*pR in the dark (*10*) and K and late M states have been reported (*11*), although N-terminal residues 1−23 and C-terminal residues 83−114 or 83−157 were missing. The crystal structure of the methylation and signaling regions has been reported for *Escherichia coli* Tsr, a member of the MCP group (*12*), although part of the methylation region was missing. Given that the primary sequences of *p*HtrII and Tsr are 26% identical, the two proteins may possess similar structures with respect to the methylation and signaling regions. Although a crystal structure of the linker region has yet to be reported, the flexible aspects of the linker region have been reported (*13*−*15*). The functional importance of the linker region in relation to signal transduction has been investigated in *p*HtrII (*16*−*18*) and other MCPs (*19*, *20*).

[†] This work was supported by grants from the Japanese Ministry of Education, Culture, Sports, Science and Technology.

[‡] The structure and NMR constraints for the *p*HtrII linker region have been deposited in the Protein Data Bank as entry 2RM8.

* To whom correspondence should be addressed. Phone: +81-743-72-5571. Fax: +81-743-72-5579. E-mail: kojima@bs.naist.jp.

[§] NAIST.

[||] Hokkaido University.

[⊥] Present address: Division of Biological Science, Graduate School of Science, Nagoya University, Chikusa-Ku, Nagoya 464-8602, Japan.

[@] Bruker Biospin K. K.

[1] Abbreviations: *p*HtrII, *pharaonis* halobacterial transducer II; *p*pR, *pharaonis* phoborhodopsin; MCPs, methyl-accepting chemotaxis proteins; HAMP, histidine kinases, adenylyl cyclases, methyl binding proteins, phosphatases; DDM, *n*-dodecyl β-D-maltoside; NMR, nuclear magnetic resonance spectroscopy; EPR, electron paramagnetic resonance spectroscopy; CD, circular dichroism; MTSL, (1-oxyl-2,2,5,5-tetramethyl-Δ3-pyrroline-3-methyl) methanethiosulfonate; PC, L-α-phosphatidylcholine; CW, continuous wave; ELDOR, electron−electron double resonance; MS, mass spectroscopy; rms, root-mean-square.

10.1021/bi701837n CCC: $37.00
Published on Web 11/15/2007

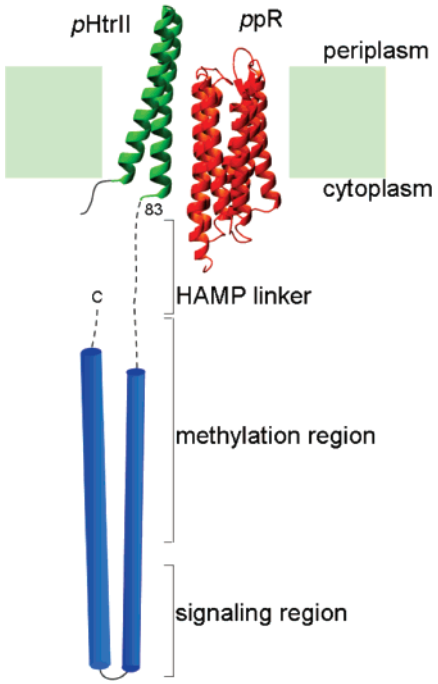

FIGURE 1: Schematic representation of *pharaonis* halobacterial transducer protein (*p*HtrII) and *pharaonis* phoborhodopsin (*pp*R) based on the crystal structures. The dashed line indicates the linker region that was the focus of this study.

The linker region contains a HAMP domain, a common structural element which has been identified by sequence comparisons and mutation analyses of sensor kinases and MCPs (*21*−*23*). Recently, the NMR structure of the HAMP domain was reported for the non-MCP protein Af1503, which was found to contain a HAMP domain as its sole cytoplasmic part (*24*). The HAMP domain consists of two helical amphipathic sequences (AS-1 and AS-2) linked by a connector sequence of undefined secondary structure. Unlike the AS-2 helix, the presence of the AS-1 helix in the *p*HtrII linker region is detected by EPR (*14*). Almost all MCPs possess a linker region comprising ca. 60 residues, although the *p*HtrII linker is twice as long as many other MCPs and its role is unknown (*21*). Long linker regions are also present in *Halobacterium salinarium* HtrI and HtrII (*25*, *26*) and are expected to play a unique role in phototactic signal transduction.

Klare et al. (*27*) reported that the structure and activity of the *p*HtrII−*pp*R complex is partly disrupted by solubilization using the mild detergent DDM and suggested the investigation of membrane-reconstituted samples. EPR provides a valuable tool for the structural investigation of proteins, and especially transmembrane proteins reconstituted into liposomes. With EPR, two electron spins interact with each other through a dipolar interaction dependent on r^{-3}, where r is the interspin distance (*28*). With the CW-EPR analysis, the relatively short distances (<20 Å) are observed as line broadenings (*28*, *29*). In pulsed ELDOR [also called double electron−electron resonance (DEER)] experiments, the longer distances of >20 Å are observed as time-dependent signal intensity modulation (*28*−*30*).

Here, the structure of the *p*HtrII linker region is investigated. Following limited proteolysis, the trypsin resistant fragment was identified as belonging to the *p*HtrII linker region. This fragment was characterized by CD, NMR, and analytical ultracentrifugation under conditions that included temperature and protein concentration as variable parameters. The high-resolution structure of this fragment was determined by NMR and further characterized by CW-EPR using detergent-solubilized and liposome-reconstituted *p*HtrII protein. Finally, the role of the linker region in signal transduction is discussed on the basis of the ELDOR data for the photoactivated *pp*R−*p*HtrII fusion protein and the structural model of the whole linker and transmembrane region of *p*HtrII complexed with *pp*R.

EXPERIMENTAL PROCEDURES

Expression and Purification of pHtrII(1−*159) Protein*. The expression plasmid of the C-terminally truncated transducer (1−159) was constructed as previously described (*31*). The protein with a C-terminal six-residue histidine tag was expressed in *E. coli* BL21(DE3) star using M9 minimal medium and purified by a previously described method with slight modifications (*31*).

Trypsin Digestion of pHtrII(1−*159) Protein and Identification of the Proteolytic Fragment*. Purified 0.48 mM *p*HtrII(1−159) protein was incubated with 1 μg/mL trypsin (Sigma) in Ni^{2+}-NTA agarose column elution buffer [Tris buffer (pH 8.5) containing 300 mM KCl, 500 mM imidazole, and 0.1% DDM] for 10 h at 4 °C. The reaction was stopped by addition of a protease inhibitor (Pefablock SC; Roche Applied Science), and the proteolytic fragment was separated by gel filtration chromatography using a HiLoad Superdex 75 column (GE Healthcare) in buffer A [10 mM citric acid buffer (pH 5.0), 50 mM KCl, and 0.1% DDM] containing 0.75 mM Pefablock SC. The proteolytic fragment was identified by N-terminal protein sequencing analysis and MALDI-TOF MS. Uniformly labeled *p*HtrII(100−159) proteolytic fragment was prepared for CD and NMR investigation.

CD Spectroscopy. Circular dichroism (CD) spectra were recorded using a J-720W CD spectropolarimeter (Jasco). The CD spectra were recorded between 200 and 260 nm [0.1 cm cell, 5 mg/mL protein in 5 mM MES buffer containing 25 mM KCl (pH 5.5)] at 0.1 nm intervals with a time constant of 4 s and a scan speed of 20 nm/min. The secondary structure was predicted using Spectra Manager, Windows version 1.0 (Jasco).

Sedimentation Equilibrium Determined by Analytical Ultracentrifugation. Sedimentation equilibrium experiments were performed using an Optima XL-A analytical ultracentrifuge (Beckman) with a four-hole An60Ti rotor at 4 °C containing six-sector cells. Concentration profiles of 20 and 800 μM ^{15}N-enriched samples in buffer B [10 mM citric acid buffer (pH 5.0) containing 50 mM KCl] were monitored by absorbance at 215 and 280 nm, respectively, at rotor speeds of 21 000, 30 000, and 39 000 rpm. The molecular weight of each sample was determined on the basis of a self-association model using Optima XL-A/XL-I data analysis software version 6.03 (Beckman). Solvent viscosity and density were calculated using SEDNTREP (J. Philo, Amgen).

NMR Spectroscopy and Structure Calculation of pHtrII(100−*159)*. Purified *p*HtrII(100−159) fragment was dissolved in buffer B containing a 90% H_2O/10% ^2H_2O mixture. NMR spectra were acquired at 277 K using a DRX800 NMR spectrometer (Bruker Biospin). Resonance assignments for

^{1}HN, ^{15}N, ^{13}Cα, ^{13}Cβ, and ^{13}C′ nuclei for the *p*HtrII(100−159) fragment were obtained from the following triple-resonance spectra applied to the ^{15}N- and ^{13}C-labeled sample: three-dimensional (3D) HNCACB, 3D HN(CO)-CACB, 3D HN(CA)CO, and 3D HNCO (*32*). Hα resonances were assigned using 3D H(CACO)NH, and side chain ^{1}H and ^{13}C resonances were assigned using 3D CCONH, 3D TOCSY-HSQC, 3D NOESY-HSQC, and 3D HCCH-TOCSY (*32*). 3D ^{15}N-edited NOESY (100 ms mixing time) and 2D ^{1}H NOESY (100 ms mixing time) were used to obtain distance restraints (*32*). All NMR spectra were processed using NMRPipe/NMRDraw (*33*) and analyzed using Sparky (*34*). ϕ and ψ angles were obtained using TALOS (*35*). CYANA version 2.1 with the CANDID protocol was used for the structure calculation (*36*). The 100 structures that were obtained were refined using AMBER version 9.0 (*37*) with a 20 ps molecular dynamics simulation using an implicit generalized Born solvent model and 1500-cycle energy minimization. The final 20 lowest-energy structures were checked using PROCHECK-NMR (*38*). All graphics were created using MOLMOL (*39*).

ppR−pHtrII(1−159) Fusion Protein Expression and Purification. PCR was used to introduce 27 nucleotides encoding a nine-residue linker [Ala-Ser-Ala-Ser-Asn-Gly-Ala-Ser-Ala (*16*) or Ala-Ser-Ala-Ser-Asn-Gly-Arg-Arg-Arg] between the C-terminal residue of *p*pR and the N-terminal residue of *p*HtrII(1−159). This fusion protein, termed *p*pR−*p*HtrII(1−159), was expressed and purified as described for the *p*HtrII(1−159) protein except for the addition of 10 mM all-*trans*-retinal during the induction.

Expression and Purification of Cysteine Mutants. For preparation of the cysteine mutants, a Quickchange site-directed mutagenesis kit (Stratagene) was used. Cysteine mutants of the *p*HtrII(1−159) and *p*pR−*p*HtrII(1−159) proteins were expressed and purified as described for the wild-type proteins except that 15 mM 2-mercaptoethanol was present during the purification.

Spin Labeling and Reconstitution in PC Liposomes. The spin-label (1-oxyl-2,2,5,5-tetramethyl-Δ3-pyrroline-3-methyl) methanethiosulfonate (MTSL; Toronto Research Chemicals Inc.) was covalently attached to cysteine residues of solubilized *p*HtrII(1−159) or *p*pR−*p*HtrII(1−159) protein according to the reported protocol (*40*). Spin-labeled proteins were checked using MS and mixed with twice the amount of nonlabeled protein. For reconstitution into L-α-phosphatidylcholine (PC), 20 mg of egg PC lipid (Avanti Polar Lipids, Inc.) was dissolved in 1 mL of chloroform, and a thin lipid film on the wall of a 5 mL flask was prepared by careful evaporation of the solvent (*41*). One milliliter of buffer A was added to the flask followed by the addition of protein to a 1:70 molar ratio of protein to lipid. Bio-Beads SM-2 Adsorbent (Bio-Rad) was added to remove the DDM, and the sample was then gently stirred overnight at 4 °C. The reconstituted protein was pelleted by centrifugation at 20000*g* for 30 min at 4 °C and then resuspended in 10 mM citric acid buffer (pH 5.0) containing 50 mM KCl or 50 mM Tris buffer (pH 7.2 for CW-EPR and pH 7.0 for pulsed ELDOR) containing 50 mM KCl.

CW-EPR Measurements. Continuous wave (CW) EPR spectra were recorded using a JES-TE300 EPR spectrometer (JEOL) at 277, 293, or 298 K, with a microwave power of 3.0 mW and a modulation amplitude of 0.1 mT. Samples were then loaded into an EPR flat cell (4.2 mm × 0.4 mm × 41.7 mm). To avoid any intermolecular effect, 1:2 labeled/unlabeled sample mixtures were used. This helps to ensure the absence or a negligible amount of doubly labeled dimer or oligomer in the sample. Solubilized samples were prepared in buffer B, and 50 mM Tris buffer (pH 7.2) containing 0.1% DDM and either 50 mM KCl, 4 M KCl, 2 M KCl and 2 M NaCl, or 4 M NaCl.

Pulsed ELDOR Measurements. Pulsed electron−electron double resonance (ELDOR) (*30*) was measured using an ELEXSYS E580 FT-EPR spectrometer fitted with a second microwave unit (Bruker Biospin). The spectrometer was equipped with a cylindrical dielectric resonator (ER4118X-MD5-W1, Bruker Biospin) and He gas flow system (CF935, Oxford Instruments). To avoid any intermolecular effect, 1:2 labeled/unlabeled sample mixtures were used. Solubilized samples were prepared in buffer B containing 10% glycerol or 50 mM Tris buffer (pH 7.0) containing 50 mM KCl, 0.1% DDM, and 10% glycerol and then loaded into EPR capillaries (3 mm inner diameter). Interspin distances were determined using simulation software (*42*).

Photoactivation of ppR. To measure the distances between the M intermediate *p*pR and *p*HtrII linker, samples were placed in an EPR cell and illuminated (Figure 1 of the Supporting Information). Illumination with >480 nm light (VY-50, Toshiba), which converted *p*pR to *p*pR$_M$, was achieved using a 1 kW halogen−tungsten lamp (Rikagakuseiki) at 253 K for 90 s (*43*). The spin-label in *p*pR at position 154 has no affect on the photocycle kinetics (*27*).

RESULTS

*Domain Identification on the pHtrII Linker Region. p*HtrII-(1−159) protein was highly expressed in *E. coli* using M9 minimal medium. The expressed protein was purified from the membrane fraction and subjected to limited proteolysis with low concentrations of trypsin at low temperatures in an effort to identify structural domains. Although *p*HtrII-(1−159) protein possesses 14 potential trypsin cleavage sites (Figure 2A), only one major band was detected by SDS−PAGE of the proteolytic products of *p*HtrII(1−159) protein (Figure 2B). The proteolytic product of *p*HtrII(1−159) protein was then subjected to N-terminal sequence and molecular weight analyses (Figure 2C). The six N-terminal amino acids of the proteolytic product were identical to residues 100−105 of *p*HtrII(1−159) protein. The molecular weight was 7939.49, as determined by MALDI-TOF MS, and is consistent with the theoretical value of 7938.43 for the *p*HtrII(100−159) fragment including the C-terminal six-residue histidine tag. Thus, it was concluded that the stable structural domain was included in the trypsin resistant fragment *p*HtrII(100−159).

Secondary Structure Analysis of the pHtrII(100−159) Fragment. CD spectra were measured in an effort to investigate the secondary structure of the digested fragment *p*HtrII(100−159). A negative band at 208 nm with a shoulder at ca. 222 nm was observed at 277 K (Figure 2 of the Supporting Information). These features are characteristic of the presence of α-helical structures. The contents of α-helix, β-sheet, turn, and random coil regions were estimated to be 40, 8, 0, and 52%, respectively. The temperature dependence of the CD spectrum was monitored at 277, 283, 293, and

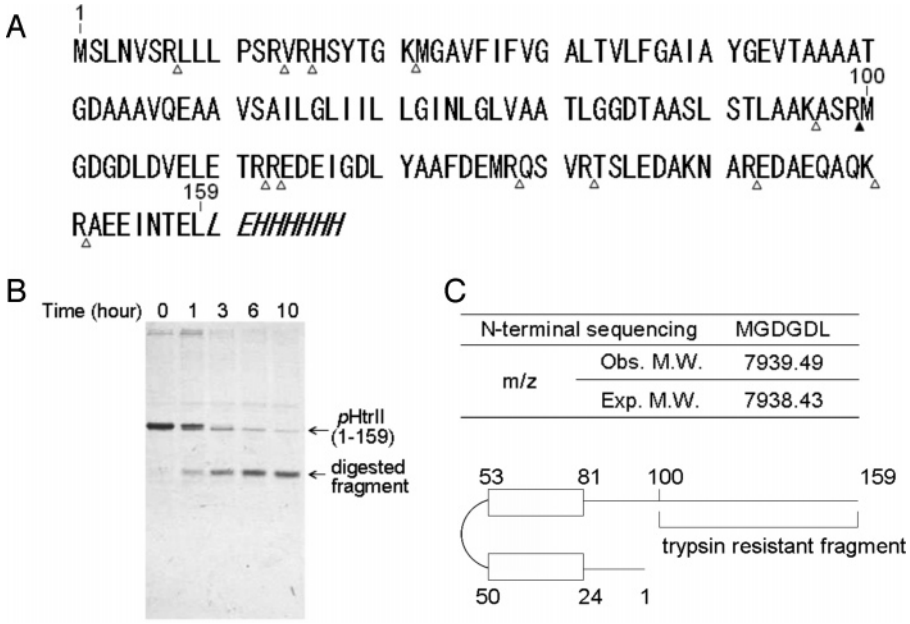

FIGURE 2: Limited trypsin digestion profile of *p*HtrII. (A) Amino acid sequence of the *p*HtrII(1−159) protein. Letters in italics refer to the six-residue histidine tag and the additional linker between the tag and the *p*HtrII(1−159) protein: (△) putative sites of trypsin cleavage and (▲) trypsin-digested site in this experiment. (B) Time course of trypsin digestion of the *p*HtrII(1−159) protein at 4 °C analyzed by SDS−PAGE. (C) Identification of the trypsin resistant fragment using MALDI-TOF MS and N-terminal protein sequencing. The digested fragment comprises residues 100−159 of *p*HtrII.

303 K (Figure 2 of the Supporting Information). The magnitude of the negative Cotton band decreased reversibly with an increase in temperature. These data indicate that the α-helical structure of the *p*HtrII(100−159) fragment is stable at low temperatures. Therefore, all subsequent experiments were carried out at 277 K, except for the pulsed ELDOR experiments.

Concentration-Dependent Dimer Formation of the pHtrII-(100−159) Fragment. $^{1}H-^{15}N$ HSQC spectra of the *p*HtrII-(100−159) fragment were measured with 20, 45, 75, 150, 300, 690, or 800 μM protein. In Figure 3A, the chemical shift differences between 20 and 690 μM samples were plotted against residue number. Although the magnitude of the difference was relatively small, the chemical shift differences were localized to residues 105−120. The semilog plots of these concentration-dependent peak shifts were sigmoidal in shape. The plot of residue R113 is shown in the inset of Figure 3A. The sigmoidal curves indicate the presence of a concentration-dependent two-state transition. Assuming a monomer−dimer equilibrium, the apparent K_d value was determined to be 115 μM.

This equilibrium was further investigated by sedimentation equilibrium analytical ultracentrifugation at low and high protein concentrations (Figure 3B and Figure 3 of the Supporting Information). As shown in Table 1, the molecular weights determined for the ^{15}N-enriched *p*HtrII(100−159) fragments were 8.1 and 17.1 ± 1.8 kDa at 20 and 800 μM, respectively. These experimental values are consistent with the theoretical molecular weights of monomer and dimer, being 8044.4 and 16 088.8 Da, respectively. Thus, it was concluded that the *p*HtrII(100−159) fragment forms a homodimer.

Determination of the Solution Structure of the pHtrII(100−159) Fragment. For the NMR structure determination, isotopically labeled recombinant *p*HtrII(1−159) protein was overexpressed in *E. coli* and purified by affinity column chromatography. Following trypsin digestion, the *p*HtrII-(100−159) fragment was purified by size exclusion and affinity column chromatography and used for 3D structure determination by solution NMR. The solution comprised buffer A without detergent since the presence of 0.1% DDM did not change the NMR spectrum. NMR resonance assignments were obtained by performing double- and triple-resonance NMR experiments using ^{15}N-labeled and ^{15}N- and ^{13}C-labeled protein samples. Almost all of the main chain and H_α resonances were assigned by conventional triple-resonance techniques, although several C_β peaks could not be detected. ^{13}C resonances of 72% of the side chains could be obtained using 3D CCONH and 3D HCCH-TOCSY, and 58% of the ^{1}H resonance assignments of the side chains, including 85% H_β and 52% H_γ, were obtained using 3D TOCSY-HSQC, 3D HCCH-TOCSY, and 3D NOESY-HSQC. Most of the sequential d_{NN} and medium-range $d_{\alpha N}(i, i + 2)$, $d_{\alpha N}(i, i + 3)$, and $d_{\alpha N}(i, i + 4)$ NOEs were manually assigned using the ^{15}N-edited NOESY spectrum. The observed medium-range NOEs indicated the presence of α-helical content in at least residues 137−147 (Figure 4A).

Unambiguous NOESY peaks were manually identified from the ^{15}N-edited NOESY spectrum and used for initial distance restraints. The dihedral angle constraints for ϕ and ψ were obtained using TALOS, which also supported the presence of α-helical content in residues 137−152. For the structure calculation, the monomer unit was used to simplify the calculation since no long-range NOE was observed. The first structure was calculated using CYANA version 2.1 and employing the CANDID protocol for ^{15}N-edited NOESY and 2D $^{1}H-^{1}H$ NOESY. The CANDID protocol provided a total of 480 distance restraints. The final structure was obtained by restrained molecular dynamics using AMBER version 9.0. Figure 4B shows the final 20 superimposed structures in ribbon representation, with disordered regions being ex-

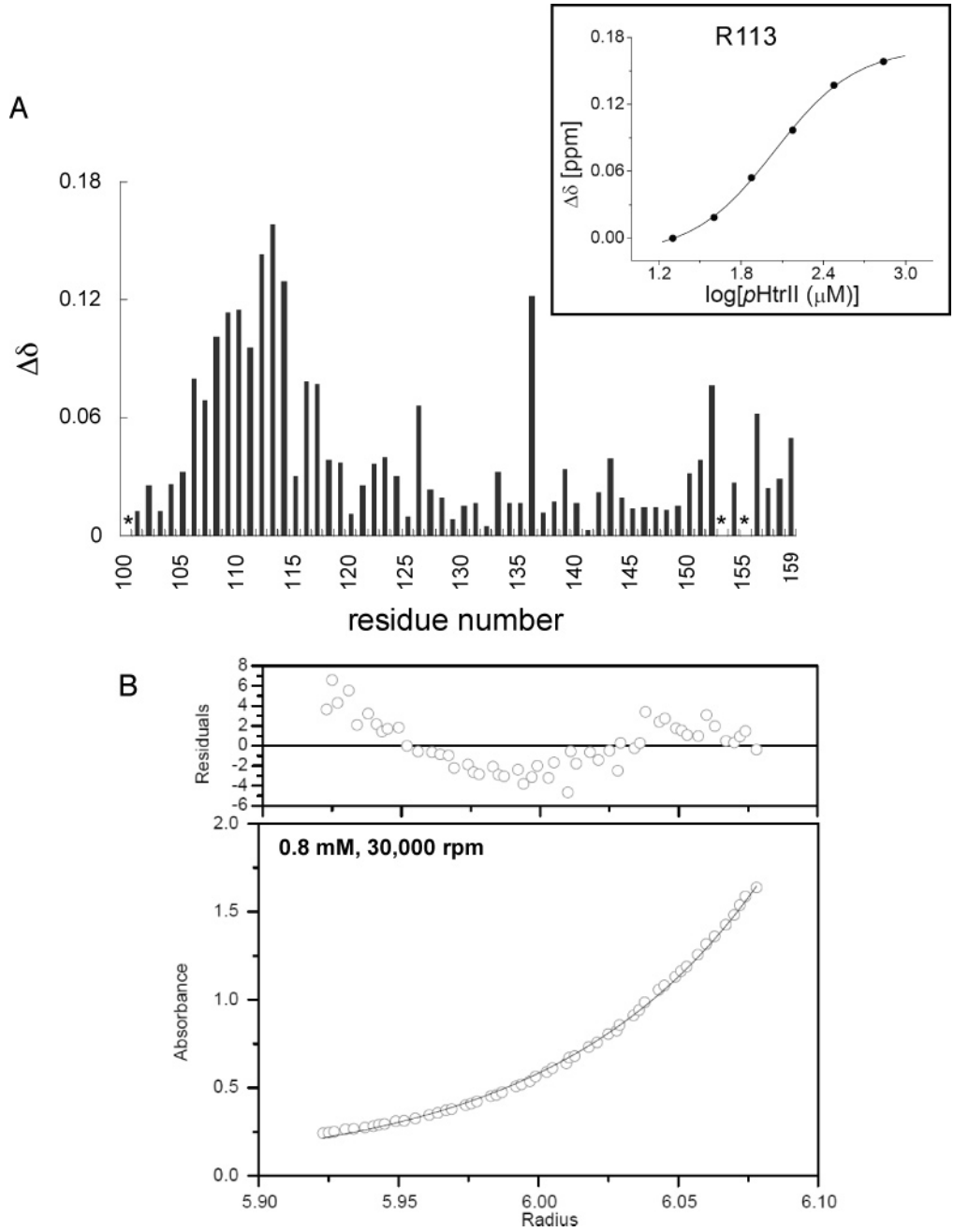

FIGURE 3: (A) Protein concentration dependence of chemical shifts of the *p*HtrII(100−159) fragment. The bars represent combined ^{1}H and ^{15}N chemical shift differences ($\Delta\delta = \{\Delta\delta(^{1}H)^2 + [\Delta\delta(^{15}N)/5]^2\}^{1/2}$) between 20 μM and 0.69 mM samples. The asterisks indicate unassigned residues. A plot of the protein concentration against $\Delta\delta$ of the R113 residue is shown in the inset. (B) Ultracentrifugation analysis of the *p*HtrII(100−159) fragment. Sedimentation equilibrium data of 0.8 mM protein are shown at a rotor speed of 30 000 rpm with the curve fitted to the self-association model.

Table 1: Molecular Weights of *p*HtrII(100−159)[a]

concentration (μM)	observed value (kDa)	calculated value (Da)
20	8.1	8044.4 (monomer)
800	17.1 ± 1.8[b]	16088.8 (dimer)

[a] Molecular weight determined by sedimentation equilibrium analytical ultracentrifugation. Calculated values for monomer and dimer are also given. For the equilibrium analysis, a total of 10 data sets were globally fitted to a self-association model at each rotor speed. [b] Averaged for three rotor speeds: 21 000, 30 000, and 39 000 rpm. The error value represents the mean error.

cluded. The final structure shows good alignment of an α-helix between residues L135 and K150. The rms deviations calculated from the averaged structure were 0.42 and 1.12 Å for backbone and heavy atoms of the converged region (residues 135−150), respectively. The statistics of the structure are given in Table 2.

Structure Analysis of Residues 135−150 of pHtrII(1−159) Protein Solubilized in DDM or Reconstituted in PC Liposomes. Residues 135−150 of the *p*HtrII(100−159) fragment formed an α-helix in water. This structure was investigated for the transmembrane protein *p*HtrII(1−159) using CW-EPR. The following single- or double-cysteine mutants of *p*HtrII(1−159) protein were prepared for the CW-EPR analysis: A145C, A141C, A138C, S134C, A145C/A141C, A145C/A138C, and A145C/S134C. The mutants were spin-labeled with MTSL at each cysteine residue. CW-EPR spectra were measured for the samples solubilized in 0.1%

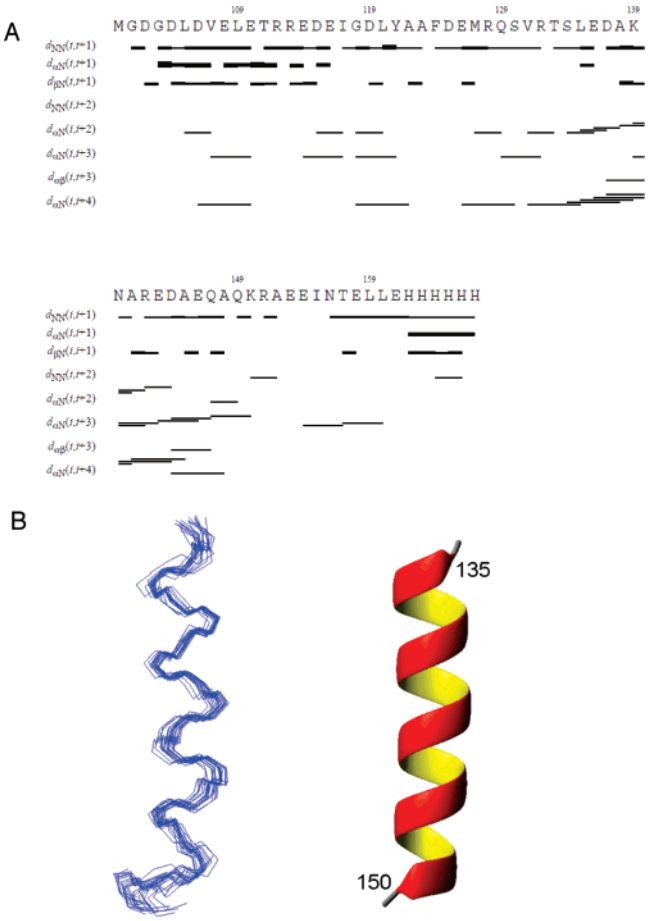

FIGURE 4: NMR structure of the *p*HtrII(100−159) fragment. (A) Summary of the sequential NOE connectivities observed for the *p*HtrII(100−159) fragment. Bars indicate NOESY cross-peaks observed between two residues. Line thickness indicates the strength of the NOE. (B) Superimposition of the 20 lowest-energy structures from the final AMBER calculations (left) and ribbon drawing of the representative structure (right).

DDM or reconstituted into PC liposomes. Figure 5 shows the spectra of the doubly labeled sample (gray line) and the summed spectra of singly labeled samples (black line). Line broadening was observed for all doubly labeled samples that had been either solubilized or reconstituted. The degree of broadening was consistent with the interspin distances of the spin-labels assuming an α-helix structure for residues 135−145 of *p*HtrII(1−159) protein. Under the presence of 1 M guanidine hydrochloride, the line broadening considerably disappeared and much sharper spectra were observed.

DISCUSSION

α-Helix Structure of Residues 135−150. In this study, the α-helix structure was determined by NMR using fragment *p*HtrII(100−159) obtained following trypsin digestion. This structure was investigated using expressed protein *p*HtrII-(100−159), the amino acid sequence of which is identical to that of the digested fragment. Surprisingly, the α-helix structure of the expressed protein was less stable than the digested fragment, as revealed by CD and NMR. The α-helix structure of the digested fragment was most stable at pH 5 at 277 K, with an α-helical content of 40%. Under the same conditions, the α-helical content of the expressed protein was 22%. In an effort to identify the presence of extraneous chemical factors that might contribute to stabilization of the α-helix in the digested fragment, further investigations were performed using NMR, MS, thin layer chromatography, and SDS−PAGE followed by silver staining. Notwithstanding the aforementioned analyses, no extraneous chemical components, such as a peptide, amino acid, or lipid component, were detected in the digested fragment sample.

Table 2: Structural Statistics for *p*HtrII(100−159)[a]

total no. of distance constraints	480
short-range ($\|i-j\| \leq 1$)	406
medium-range ($\|i-j\| < 5$)	74
long-range ($\|i-j\| \geq 5$)	0
no. of dihedral constraints (ϕ, φ)	22, 22
no. of hydrogen bonds	9
rms deviation from experimental constraints[b]	
distances (Å)	0.123 ± 0.057
angles (deg)	1.544 ± 0.207
rms deviation from idealized covalent geometry	
bonds (Å)	0.0101 ± 0.0001
angles (deg)	2.509 ± 0.028
AMBER energy terms (kcal/mol)	
E_{amber}	−3229 ± 16
van der Waals energy	−365 ± 12
electrostatic energy	−3892 ± 130
constraint energy	5 ± 1
Ramachandran plot[c] (residues 135−150)	
residues in most favored regions (%)	99.4
residues in additionally allowed regions (%)	0.6
residues in generously allowed regions (%)	0.0
residues in disallowed regions (%)	0.0
rms deviation of mean structure derived from 20 calculated structures	
backbone atoms (residues 135−150) (Å)	0.42 ± 0.17
all heavy atoms (residues 135−150) (Å)	1.12 ± 0.12

[a] These statistics comprise an ensemble of the 20 lowest-energy structures obtained from 100 starting structures. The structure was determined using CYANA version 2.1 with the CANDID protocol and refined using AMBER version 9.0. [b] None of these structures exhibited distance violations of >0.5 Å or dihedral angle violations of >5°. [c] Determined using PROCHECK.

The presence of an α-helix within the transmembrane protein *p*HtrII(1−159) was confirmed using EPR at pH 5 and 277 K (Figure 5). At pH 7.2 and 298 K, dipolar broadening was observed for both the solubilized and reconstituted samples (Figure 6), although the degree of broadening decreased slightly compared to that of the spectra measured at pH 5.0 and 277 K. It was noted that the α-helical content of digested fragment *p*HtrII(100−159) almost disappeared at 298 K (Figure 2 of the Supporting Information). These results indicate that the α-helix found within the digested fragment is significantly stabilized within transmembrane protein *p*HtrII(1−159), possibly because of the homodimer stabilization via the transmembrane region.

Structure of pHtrII(1−159) Linker Region Residues 100−134. α-Helical content is present only between residues 135 and 150 of the *p*HtrII(100−159) fragment. Only one major trypsin resistant fragment, *p*HtrII(100−159), was detected, although there are four potential trypsin cleavage sites that lie between residues 100 and 134 (Figure 2A). This resistance to trypsin digestion indicates the presence of protection factors located between residues 100 and 134, which might be related to the unique structure formed between residues 100 and 134 and/or intermolecular association. The former possibility is suggested by the experimental data.

The α-helical content of 40%, determined by CD analysis, is significantly higher than the 24% α-helical content calculated from the NMR structure. The chemical shift values

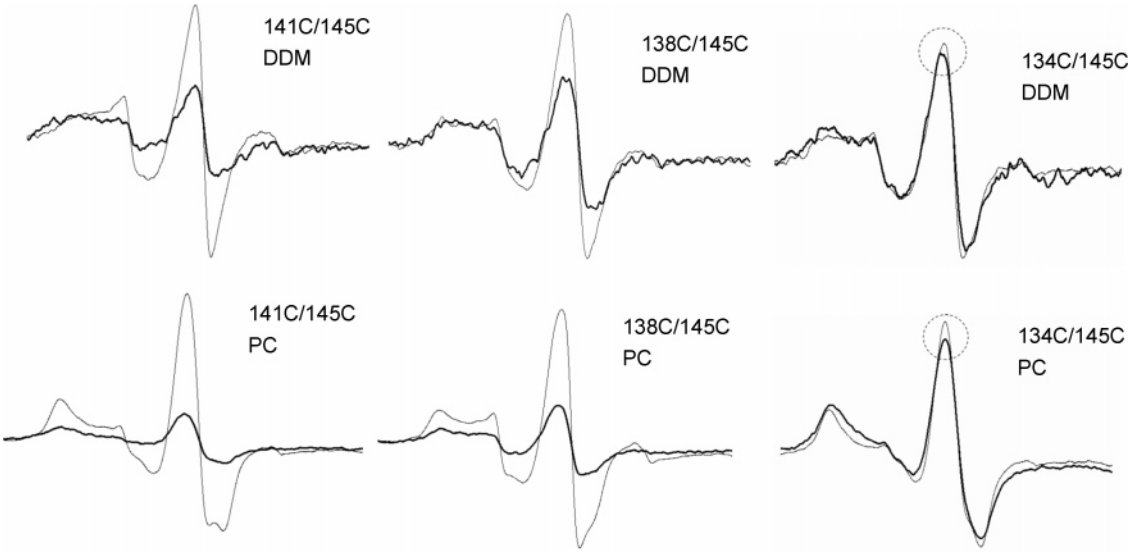

FIGURE 5: CW-EPR spectra of the *p*HtrII(1−159) protein at 277 K. 134C, 138C, 141C, and 145C refer to the spin-labeled positions. DDM and PC refer to the solubilized sample in 0.1% DDM and the reconstituted sample in PC liposomes, respectively. The summed spectra of two singly labeled samples (gray) and the spectrum of a doubly labeled sample (black) are superimposed.

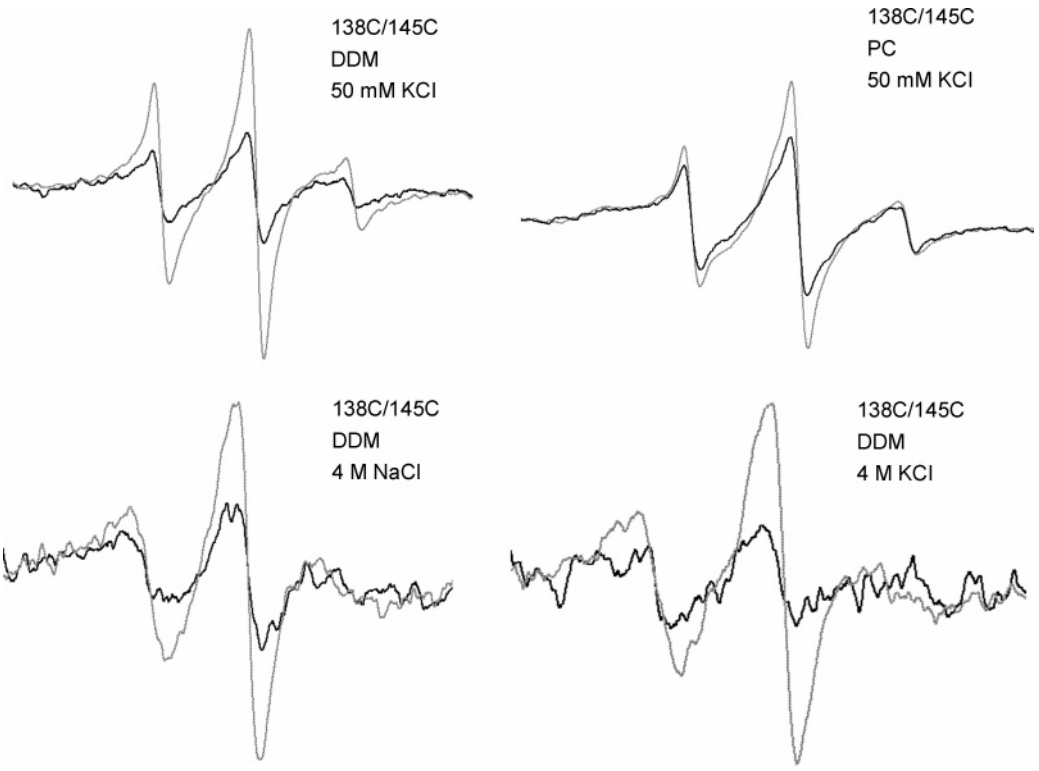

FIGURE 6: CW-EPR spectra of the *p*HtrII(1−159) protein in Tris buffer (pH 7.2) at 298 K. Salt conditions are shown on the right shoulder of each spectrum. 134C, 138C, 141C, and 145C refer to the spin-labeled positions. DDM and PC refer to the solubilized sample in 0.1% DDM and the reconstituted sample in PC liposomes, respectively. The summed spectra of two singly labeled samples (gray) and the spectrum of a doubly labeled sample (black) are superimposed.

and some NOE data suggest the formation of helical structure between residues 100 and 134. Thus, it is reasonable to assume that the structure adopted by residues 100−134 represents an unstable α-helix or a discontinuous α-helix. Presumably this α-helix is stabilized within the transmembrane protein *p*HtrII, such as with the α-helix located between residues 135−150 shown here, and with stabilization of the α-helix of the EnvZ HAMP domain in the presence of domain A (*44*). The presence of intermolecular association is clear since the digestion experiment was performed using 0.48 mM protein, a concentration much higher than the K_d value of dimer formation, 115 μM. However, it remains unclear whether dimer formation can protect the protein from trypsin digestion or if residues 100−134 can indeed form a dimer interface.

Dimer Interface of the pHtrII(100−159) Fragment. The trypsin-digested fragment *p*HtrII(100−159) forms a homodimer as determined by analytical ultracentrifugation (Figure 3). Significant NMR chemical shift changes upon dimer formation are localized to residues 105−120. Chemical shift changes are related changes in chemical environment, such as those occurring at an interaction interface or

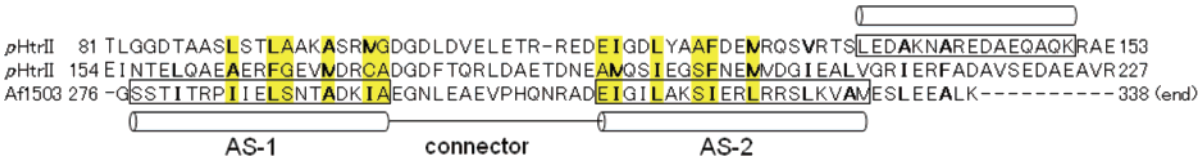

FIGURE 7: Sequence alignment of *p*HtrII and the *Archaeoglobus fulgidus* Af1503 HAMP domain. Hydrophobic residues in heptad repeats are shown in bold. The helix structure determined in this investigation (*p*HtrII) and that previously reported (Af1503) (*24*) are boxed in black. Important regions involved in packing interactions in Af1503 are highlighted in yellow.

manifested by a conformational change. Thus, the dimer interface and/or the conformational change induced by dimer formation is localized to residues 105−120. The intermolecular interaction affects NMR signals as the chemical shift changes and/or line broadening occurs. Since no sequence-specific line broadening was observed upon dimer formation, we can conclude that the dimer interface is localized to residues 105−120. This conclusion is consistent with previously reported EPR results showing close contacts between residues 115 and 115 (interdimer) and residues 122 and 122 (interdimer) (*14*). The presence of induced conformational change remains uncertain due to a lack of data. The apparent disagreement between the NMR structure and the limited digestion data can be explained by the presence of an unstable α-helix between residues 100 and 134 and dimer formation involving residues 105−120.

HAMP Domain in pHtrII. A HAMP domain is found in the *p*HtrII linker region and consists of two helices, AS-1 and AS-2, located between residues 83 and 100 and residues 117 and 131, respectively (*14*). The solution structure of the Af1503 HAMP domain was recently determined (*24*). Sequence alignment of the *p*HtrII linker region and Af1503 HAMP domain was performed using CLUSTALW (Figure 7). On the basis of the secondary structure of Af1503, the first and second helices were estimated to be located between residues 83 and 102 and residues 115 and 136, respectively, and the HAMP domain was localized to residues 83−136. In Figure 7, another HAMP domain is shown in the *p*HtrII linker region. On the basis of the secondary structure of Af1503, the first and second helices of the second HAMP domain were estimated to be located between residues 157 and 176 and residues 190 and 211, respectively, and the second HAMP domain was localized to residues 157−211 of *p*HtrII. Using PROSITE (*45*−*48*), these two HAMP domains within the linker region were also found as the first and second HAMP domains located between residues 84 and 136 and residues 157 and 210, respectively.

In this study, only one α-helix, located between residues 135 and 150, was determined for the digested fragment *p*HtrII(100−159). This region lies outside of the HAMP domain, and no clear structure is observed within the HAMP domain. However, as discussed above, the structure adopted by residues 100−134 of the HAMP domain is assumed to be that of an unstable α-helix. Moreover, residues 105−120 represent the dimer interface of the digested fragment. These characteristic features are consistent with those of the HAMP domain. Assuming a four-helix bundle structure for the first HAMP domain, the presence of an unstable α-helix located between residues 100 and 134 can easily be ascribed to the absence of the first helix in the first HAMP domain.

The structure of the HAMP domain was examined by the pulsed electron−electron double-resonance (ELDOR) method using the *pp*R−*p*HtrII(1−159) fusion proteins ppR_{S154C}−*p*HtrII(1−159)$_{S98C}$ and ppR_{S154C}−*p*HtrII(1−159)$_{S134C}$ with an MTSL spin-label at each cysteine residue (Figure 8). The distances between the *pp*R E−F loop and the *p*HtrII linker region are listed in Table 3. The ppR_{154}−$pHtrII_{98}$ distance of ∼20 Å for the PC-reconstituted sample is slightly shorter than that expected from the reported values (*14*). The

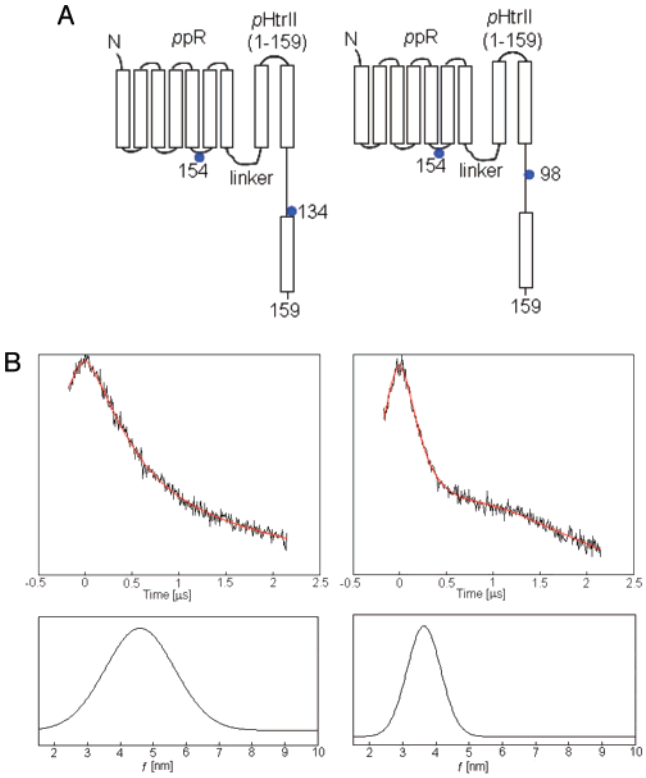

FIGURE 8: Interspin distance measurement using ELDOR. (A) Schematic representation of spin-labeled residues ppR_{154} and $pHtrII_{98}$ or $pHtrII_{134}$. Distances between ppR_{154} and $pHtrII_{98}$ or $pHtrII_{134}$ were determined. (B) ELDOR time traces (black line) and simulated spectra (red line) are shown in the top panels with distance distribution data (bottom panels).

Table 3: Interspin Distances between *pp*R and the *p*HtrII Linker[a]

*p*HtrII position	interspin distance (Å)			
	pH 5.0 (dark)	pH 5.0 (dark)[f]	pH 7.0 (dark)	pH 7.0 (light)
98[b]	36.4 ± 3.6[d]	35.1 ± 4.5[d]	37.2 ± 3.4[d]	36.8 ± 4.0[d]
98[c]	20.2 ± 4[d]	19.7 ± 5.4[d]	21.3 ± 3.2[d]	22.2 ± 2.6[d]
134[b]	46.0 ± 7.5[d]	42.9 ± 7.8[d]	47.8 ± 7.4[d]	47.2 ± 7.2[d]
134[c]	ND[e]	ND[e]	ND[e]	ND[e]

[a] Interspin distances of the *pp*R−*p*HtrII fusion protein between *pp*R (position 154) and *p*HtrII (position 98 or 134) determined using the pulsed ELDOR method. [b] Solubilized by DDM. [c] Reconstituted in phosphatidylcholine. [d] The deviation represents the experimental error as a Gaussian peak width. [e] Not determined. [f] The *pp*R−*p*HtrII fusion protein with a different linker sequence (ASASNGRRR) between *pp*R and *p*HrII.

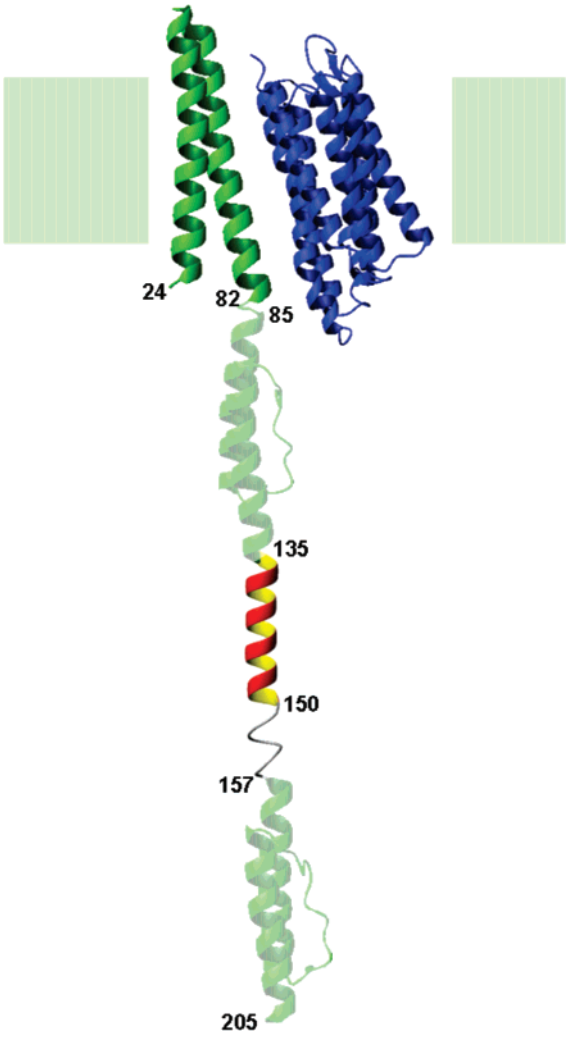

FIGURE 9: Modeled structure of the *p*HtrII linker region in the *p*pR−*p*HtrII complex. Crystal structures of *p*pR and the transmembrane region of *p*HtrII (PDB entry 1H2S) are colored blue and green, respectively. The NMR structure of the joint helix of *p*HtrII (PDB entry 2RM8) is colored red and yellow. The modeled structures of two HAMP domains of *p*HtrII generated by homology modeling using MODELLER and based on the NMR structure of Af1503 (PDB entry 2ASX) are colored light green.

*p*pR$_{154}$−*p*HtrII$_{98}$ distance of ∼35 Å for the DDM-solubilized sample was much longer than that of the reconstituted sample. These distances were independent of pH and linker sequence between *p*pR and *p*HtrII. This difference in distance between the solubilized and reconstituted samples may support the proposition that the detergent-solubilized structure is impaired in the juxtamembrane region (*27*). The *p*pR$_{154}$−*p*HtrII$_{134}$ distance for the PC-reconstituted sample was not determined due to the fast electron spin relaxation. The *p*pR$_{154}$−*p*HtrII$_{134}$ distance of ∼45 Å for the DDM-solubilized sample was much shorter than that of the extended structure and suggests the presence of a folded structure. Although ELDOR analysis could not clarify the detailed structure of the HAMP domain, these data suggest the presence of some distinct structure, such as a four-helix bundle.

Role of the α*-Helix Located between Residues 135 and 150 in Signal Transduction.* The α-helix structure between residues 135 and 150 determined in this report together with the crystal structure of the *p*pR−*p*HtrII complex and the modeled structures of two HAMP domains are shown in Figure 9. The HAMP domain structures were generated on the basis of the structure of the Af1503 HAMP domain using MODELLER (*49*). The *p*pR$_{154}$−*p*HtrII$_{98}$ and *p*pR$_{154}$−*p*HtrII$_{134}$ distances of the modeled structure shown in Figure 9 are ca. 20 and 35 Å, respectively. The *p*pR$_{154}$−*p*HtrII$_{98}$ distance is in good agreement with our ELDOR data for the PC-reconstituted sample (Table 3). The α-helix located between residues 135 and 150 is a direct continuation of the second helix of the first HAMP domain which connects the second HAMP domain. More specifically, the α-helix located between residues 135 and 150 may function as a mechanical joint helix between the two HAMP domains to transfer rotational motion.

Finally, the light-induced structural change was monitored by the ELDOR method. The interspin distances of the activated state were measured at pH 7.0 since the absorption maxima of *p*pR remained unchanged following illumination with >480 nm light at pH 5.0. As shown in Table 3, no significant distance change was observed, although a slight increase was recorded for the *p*pR$_{154}$−*p*HtrII$_{98}$ distance within the error bar. These data suggest that the large structural change of >3 Å is not induced in photoactivated signal transduction. This is in good agreement with previous structural studies (*11*, *24*) and FRET analysis (*50*) where a 15° clockwise rotation with a 0.9 Å displacement of TM2 and a 0.3−0.8 Å movement of the linker region were observed. To transmit these small conformational changes, the structure of the transducer should be relatively rigid. The modeled structure shown in Figure 9 can transmit such small motion mechanically and, thus, facilitate signal transduction.

CONCLUSION

In this report, the structure of the *p*HtrII linker region was investigated biochemically and biophysically. The trypsin resistant fragment *p*HtrII(100−159) within the linker region contains ∼40% α-helical content and forms a homodimer with a K_d value of 115 μM. The NMR structure of the *p*HtrII-(100−159) fragment reveals the presence of an α-helix located between residues 135 and 150. This α-helix is significantly stabilized within the transmembrane protein *p*HtrII(1−159). Sequence alignment suggests the presence of two HAMP domains located between residues 83 and 136 and residues 157 and 211. The presence of an unstable α-helix between residues 100 and 134 and the dimer interface between residues 105 and 120 are consistent with formation of an Af1503 HAMP domainlike structure. The *p*pR$_{154}$−*p*HtrII$_{98}$ distance determined by ELDOR for the PC-reconstituted sample is in good agreement with the modeled structure based on the Af1503 HAMP domainlike structure. The light-activated *p*pR$_{154}$−*p*HtrII$_{98}$ change in distance is <3 Å. The α-helix located between residues 135 and 150 as determined in this report may function as a mechanical joint between two HAMP domains to transmit the photoactivated small motion that facilitates signal transduction.

ACKNOWLEDGMENT

We thank Prof. Toshio Hakoshima (NAIST) for help with use of the analytical centrifuge, Ms. Hiroko Kinoshita for help in the preparation of expression plasmids, Ms. Junko Tsukamoto for technical assistance with mass spectroscopy and N-terminal protein sequencing, and Prof. Yuji Kobayashi

(Osaka University of Pharmaceutical Sciences, Osaka, Japan) for helpful comments.

SUPPORTING INFORMATION AVAILABLE

Detailed methods for sample preparation and three figures of the photoactivation of *p*pR−*p*HtrII fusion protein sample, CD spectra of the *p*HtrII(100−159) fragment, and ultracentrifugation analysis data. This material is available free of charge via the Internet at http://pubs.acs.org.

REFERENCES

1. Rudolph, J., Nordmann, B., Storch, K. F., Gruenberg, H., Rodewald, K., and Oesterhelt, D. (1996) A family of halobacterial transducer proteins, *FEMS Microbiol. Lett. 139*, 161−168.
2. Falke, J. J., and Hazelbauer, G. L. (2001) Transmembrane signaling in bacterial chemoreceptors, *Trends Biochem. Sci. 26*, 257−265.
3. Rudolph, J., and Oesterhelt, D. (1996) Deletion analysis of the che operon in the archaeon *Halobacterium salinarium*, *J. Mol. Biol. 258*, 548−554.
4. Alley, M. R., Maddock, J. R., and Shapiro, L. (1993) Requirement of the carboxyl terminus of a bacterial chemoreceptor for its targeted proteolysis, *Science 259*, 1754−1757.
5. Maddock, J. R., and Shapiro, L. (1993) Polar location of the chemoreceptor complex in the *Escherichia coli* cell, *Science 259*, 1717−1723.
6. Zhang, X. N., Zhu, J., and Spudich, J. L. (1999) The specificity of interaction of archaeal transducers with their cognate sensory rhodopsins is determined by their transmembrane helices, *Proc. Natl. Acad. Sci. U.S.A. 96*, 857−862.
7. Spudich, J. L., Yang, C. S., Jung, K. H., and Spudich, E. N. (2000) Retinylidene proteins: Structures and functions from archaea to humans, *Annu. Rev. Cell Dev. Biol. 16*, 365−392.
8. Yan, B., Takahashi, T., Johnson, R., and Spudich, J. L. (1991) Identification of signaling states of a sensory receptor by modulation of lifetimes of stimulus-induced conformations: The case of sensory rhodopsin II, *Biochemistry 30*, 10686−10692.
9. Klare, J. P., Gordeliy, V. I., Labahn, J., Büldt, G., Steinhoff, H. J., and Engelhard, M. (2004) The archaeal sensory rhodopsin II/transducer complex: A model for transmembrane signal transfer, *FEBS Lett. 564*, 219−224.
10. Gordeliy, V. I., Labahn, J., Moukhametzianov, R., Efremov, R., Granzin, J., Schlesinger, R., Büldt, G., Savopol, T., Scheidig, A. J., Klare, J. P., and Engelhard, M. (2002) Molecular basis of transmembrane signalling by sensory rhodopsin II-transducer complex, *Nature 419*, 484−487.
11. Moukhametzianov, R., Klare, J. P., Efremov, R., Baeken, C., Göppner, A., Labahn, J., Engelhard, M., Büldt, G., and Gordeliy, V. I. (2006) Development of the signal in sensory rhodopsin and its transfer to the cognate transducer, *Nature 440*, 115−119.
12. Kim, K. K., Yokota, H., and Kim, S. H. (1999) Four-helical-bundle structure of the cytoplasmic domain of a serine chemotaxis receptor, *Nature 400*, 787−792.
13. Sudo, Y., Okuda, H., Yamabi, M., Fukuzaki, Y., Mishima, M., Kamo, N., and Kojima, C. (2005) Linker region of a halobacterial transducer protein interacts directly with its sensor retinal protein, *Biochemistry 44*, 6144−6152.
14. Bordignon, E., Klare, J. P., Doebber, M., Wegener, A. A., Martell, S., Engelhard, M., and Steinhoff, H. J. (2005) Structural analysis of a HAMP domain: The linker region of the phototransducer in complex with sensory rhodopsin II, *J. Biol. Chem. 280*, 38767−38775.
15. Budyak, I. L., Pipich, V., Mironova, O. S., Schlesinger, R., Zaccai, G., and Klein-Seetharaman, J. (2006) Shape and oligomerization state of the cytoplasmic domain of the phototaxis transducer II from *Natronobacterium pharaonis*, *Proc. Natl. Acad. Sci. U.S.A. 103*, 15428−15433.
16. Jung, K. H., Spudich, E. N., Trivedi, V. D., and Spudich, J. L. (2001) An archaeal photosignal-transducing module mediates phototaxis in *Escherichia coli*, *J. Bacteriol. 183*, 6365−6371.
17. Yang, C. S., and Spudich, J. L. (2001) Light-induced structural changes occur in the transmembrane helices of the *Natronobacterium pharaonis* HtrII transducer, *Biochemistry 40*, 14207−14214.
18. Yang, C. S., Sineshchekov, O., Spudich, E. N., and Spudich, J. L. (2004) The cytoplasmic membrane-proximal domain of the HtrII transducer interacts with the E-F loop of photoactivated *Natronomonas pharaonis* sensory rhodopsin II, *J. Biol. Chem. 279*, 42970−42976.
19. Umemura, T., Matsumoto, Y., Ohnishi, K., Homma, M., and Kawagishi, I. (2002) Sensing of cytoplasmic pH by bacterial chemoreceptors involves the linker region that connects the membrane-spanning and the signal-modulating helices, *J. Biol. Chem. 277*, 1593−1598.
20. Appleman, J. A., and Stewart, V. (2003) Mutational analysis of a conserved signal-transducing element: The HAMP linker of the *Escherichia coli* nitrate sensor NarX, *J. Bacteriol. 185*, 89−97.
21. Le Moual, H., and Koshland, D. E., Jr. (1996) Molecular Evolution of the C-terminal Cytoplasmic Domain of a Superfamily of Bacterial Receptors Involved in Taxis, *J. Mol. Biol. 261*, 568−585.
22. Aravind, L., and Ponting, C. P. (1999) The cytoplasmic helical linker domain of receptor histidine kinase and methyl-accepting proteins is common to many prokaryotic signalling proteins, *FEMS Microbiol. Lett. 176*, 111−116.
23. Williams, S. B., and Stewart, V. (1999) Functional similarities among two-component sensors and methyl-accepting chemotaxis proteins suggest a role for linker region amphipathic helices in transmembrane signal transduction, *Mol. Microbiol. 33*, 1093−1102.
24. Hulko, M., Berndt, F., Gruber, M., Linder, J. U., Truffault, V., Schultz, A., Martin, J., Schultz, J. E., Lupas, A. N., and Coles, M. (2006) The HAMP domain structure implies helix rotation in transmembrane signaling, *Cell 126*, 929−940.
25. Yao, V. J., and Spudich, J. L. (1992) Primary structure of an archaebacterial transducer, a methyl-accepting protein associated with sensory rhodopsin I, *Proc. Natl. Acad. Sci. U.S.A. 89*, 11915−11919.
26. Zhang, W., Brooun, A., Mueller, M. M., and Alam, M. (1996) The primary structures of the Archaeon *Halobacterium salinarium* blue light receptor sensory rhodopsin II and its transducer, a methyl-accepting protein, *Proc. Natl. Acad. Sci. U.S.A. 93*, 8230−8235.
27. Klare, J. P., Bordignon, E., Doebber, M., Fitter, J., Kriegsmann, J., Chizhov, I., Steinhoff, H. J., and Engelhard, M. (2006) Effects of solubilization on the structure and function of the sensory rhodopsin II/transducer complex, *J. Mol. Biol. 356*, 1207−1221.
28. Rabenstein, M. D., and Shin, Y. K. (1995) Determination of the distance between two spin labels attached to a macromolecule, *Proc. Natl. Acad. Sci. U.S.A. 92*, 8239−8243.
29. Altenbach, C., Oh, K. J., Trabanino, R. J., Hideg, K., and Hubbell, W. L. (2001) Estimation of inter-residue distances in spin labeled proteins at physiological temperatures: Experimental strategies and practical limitations, *Biochemistry 40*, 15471−15482.
30. Pannier, M., Veit, S., Godt, A., Jeschke, G., and Spiess, H. W. (2000) Dead-time free measurement of dipole-dipole interactions between electron spins, *J. Magn. Reson. 142*, 331−340.
31. Sudo, Y., Iwamoto, M., Shimono, K., and Kamo, N. (2001) *Pharaonis* Phoborhodopsin Binds to its Cognate Truncated Transducer Even in the Presence of a Detergent with a 1:1 Stoichiometry, *Photochem. Photobiol. 74*, 489−494.
32. Cavanagh, J., Fairbrother, W. J., Palmer, A. G., and Skelton, N. J. (1996) *Protein NMR Spectroscopy*, Academic Press, San Diego.
33. Delaglio, F., Grzesiek, S., Vuister, G. W., Zhu, G., Pfeifer, J., and Bax, A. (1995) NMRPipe: A multidimensional spectral processing system based on UNIX pipes, *J. Biomol. NMR 6*, 277−293
34. Goddard, T. D., and Kneller, D. G. (1999) *SPARKY3*, University of California, San Francisco.
35. Cornilescu, G., Delaglio, F., and Bax, A. (1999) Protein backbone angle restraints from searching a database for chemical shift and sequence homology, *J. Biomol. NMR 13*, 289−302.
36. Herrmann, T., Güntert, P., and Wüthrich, K. (2002) Protein NMR structure determination with automated NOE assignment using the new software CANDID and the torsion angle dynamics algorithm DYANA, *J. Mol. Biol. 319*, 209−227.
37. Pearlman, D. A., Case, D. A., Caldwell, J. W., Ross, W. S., Cheatham, T. E. I., DeBolt, S., Ferguson, D., Seibel, G., and Kollman, P. (1995) AMBER, a package of computer programs for applying molecular mechanics, normal mode analysis, molecular dynamics and free energy calculations to simulate the structural and energetic properties of molecules, *Comput. Phys. Commun. 91*, 1−41.
38. Laskowski, R. A., Rullmannn, J. A., MacArthur, M. W., Kaptein, R., and Thornton, J. M. (1996) AQUA and PROCHECK-NMR:

Programs for checking the quality of protein structures solved by NMR, *J. Biomol. NMR 8*, 477−486.
39. Koradi, R., Billeter, M., and Wüthrich, K. (1996) MOLMOL: A program for display and analysis of macromolecular structures, *J. Mol. Graphics 14*, 51−55, 29−32.
40. Pfeiffer, M., Rink, T., Gerwert, K., Oesterhelt, D., and Steinhoff, H. J. (1999) Site-directed Spin-labeling Reveals the Orientation of the Amino Acid Side-chains in the E-F Loop of Bacteriorhodopsin, *J. Mol. Biol. 287*, 163−171.
41. Kandori, H., Shimono, K., Sudo, Y., Iwamoto, M., Shichida, Y., and Kamo, N. (2001) Structural changes of *pharaonis* phoborhodopsin upon photoisomerization of the retinal chromophore: Infrared spectral comparison with bacteriorhodopsin, *Biochemistry 40*, 9238−9246.
42. Pannier, M., Veit, S., Schöps, M., Wiesner, U., Jeschke, G., and Spiess, H. W. (2000) Determination of ion cluster sizes and cluster-to-cluster distances in ionomers by four-pulse double electron electron resonance spectroscopy, *Macromolecules 33*, 7812−7818.
43. Furutani, Y., Kamada, K., Sudo, Y., Shimono, K., Kamo, N., and Kandori, H. (2005) Structural changes of the complex between *pharaonis* phoborhodopsin and its cognate transducer upon formation of the M photointermediate, *Biochemistry 44*, 2909−2915.
44. Kishii, R., Falzon, L., Yoshida, T., Kobayashi, H., and Inouye, M. (2007) Structural and functional studies of the HAMP domain of EnvZ, an osmosensing transmembrane histidine kinase in *Escherichia coli*, *J. Biol. Chem.* (in press).
45. Hulo, N., Bairoch, A., Bulliard, V., Cerutti, L., De Castro, E., Langendijk-Genevaux, P. S., Pagni, M., and Sigrist, C. J. A. (2006) The PROSITE database, *Nucleic Acids Res. 34*, D227−D230.
46. Sigrist, C. J. A., Cerutti, L., Hulo, N., Gattiker, A., Falquet, L., Pagni, M., Bairoch, A., and Bucher, P. (2002) PROSITE: A documented database using patterns and profiles as motif descriptors, *Briefings Bioinf. 3*, 265−274.
47. Gattiker, A., Gasteiger, E., and Bairoch, A. (2002) ScanProsite: A reference implementation of a PROSITE scanning tool, *Appl. Bioinf. 1*, 107−108.
48. Sigrist, C. J. A., De Castro, E., Langendijk-Genevaux, P. S., Le Saux, V., Bairoch, A., and Hulo, N. (2005) ProRule: A new database containing functional and structural information on PROSITE profiles, *Bioinformatics 21*, 4060−4066.
49. Sali, A., and Blundell, T. L. (1993) Comparative protein modelling by satisfaction of spatial restraints, *J. Mol. Biol. 234*, 779−815.
50. Taniguchi, Y., Ikehara, T., Kamo, N., Yamasaki, H., and Toyoshima, T. (2007) Dynamics of light-induced conformational changes of the phoborhodopsin/transducer complex formed in the *n*-dodecyl *β*-D-maltoside micelle, *Biochemistry 46*, 5349−5357.

BI701837N